

Nonreciprocal phase shift within zeptosecond temporal scale

Xiao Han(韩啸) and Shuai Ben(贲帅)

Citation: Chin. Phys. B, 2025, 34 (**10**): 104201. DOI: 10.1088/1674-1056/adf1e8
http://cpb.iphy.ac.cn; http://iopscience.iop.org/cpb

What follows is a list of articles you may be interested in

Generation ofWatt-level Kerr-lens mode-locked Yb:CYA laser at 1-GHz repetition rate

Guodong Zhao(赵国栋), Junyi Ma(马骏逸), Hainian Han(韩海年), Zhaohua Wang(王兆华), and Zhiyi Wei(魏志义)
Chin. Phys. B, 2025, 34 (**8**): 084204. DOI: 10.1088/1674-1056/adcf8b

Third-order nonlinear wavelength conversion in chalcogenide glass waveguides towards mid-infrared photonics

Fengbo Han(韩锋博), Jiaxin Gu(顾佳新), Lu Huang(黄璐), Hang Wang(王航), Yali Huang(黄雅莉), Xuecheng Zhou(周学成), Shaoliang Yu(虞绍良), Zhengqian Luo(罗正钱), Zhipeng Dong(董志鹏), and Qingyang Du(杜清扬)
Chin. Phys. B, 2024, 33 (**10**): 104207. DOI: 10.1088/1674-1056/ad6557

Terahertz shaping technology based on coherent beam combining

Xiao-Ran Zheng(郑晓冉), Dan-Ni Ma(马丹妮), Guang-Tong Jiang(蒋广通), Cun-Lin Zhang(张存林), and Liang-Liang Zhang(张亮亮)
Chin. Phys. B, 2023, 32 (**11**): 114210. DOI: 10.1088/1674-1056/acc2b0

A 45-μJ, 10-kHz, burst-mode picosecond optical parametric oscillator synchronously pumped at a second harmonic cavity

Chao Ma(马超), Ke Liu(刘可), Yong Bo(薄勇), Zhi-Min Wang(王志敏), Da-Fu Cui(崔大复), and Qin-Jun Peng(彭钦军)
Chin. Phys. B, 2022, 31 (**8**): 084206. DOI: 10.1088/1674-1056/ac6016

Ultrafast plasmon dynamics in asymmetric gold nanodimers

Bereket Dalga Dana, Alemayehu Nana Koya, Xiaowei Song(宋晓伟), and Jingquan Lin(林景全)
Chin. Phys. B, 2022, 31 (**6**): 064208. DOI: 10.1088/1674-1056/ac3737

SPECIAL TOPIC — Ultrafast physics in atomic, molecular and optical systems

Nonreciprocal phase shift within zeptosecond temporal scale

Xiao Han(韩啸)[1] and Shuai Ben(贲帅)[2,†]

[1] *Jilin Vocational College of Industry and Technology, Jilin* 132013, *China*
[2] *School of Physics and Optoelectronic Engineering, Hainan University, Haikou* 570228, *China*

(Received 14 May 2025; revised manuscript received 4 July 2025; accepted manuscript online 19 July 2025)

We investigate the zeptosecond-timescale delayed ionization process induced by ultrafast laser propagation in different directions across the molecule. The experimental measurements by Grundmann *et al*. [*Science* **370** 339 (2020)] serve as a basis for our study, where they extract the birth time delay of photoelectron emission from two nuclei, amounting to a few hundred zeptoseconds. By comparing and analyzing the results, we observe that asymmetric systems, such as the $2p\sigma$ state of HeH^{2+}, exhibit nonequivalent responses to forward and backward laser propagation, resulting in an asymmetric dependence of the interference structure in the photoelectron momentum spectra. This process is considered as an ultrafast nonreciprocal phase shift with zeptosecond resolution. Through computational simulations, we explore the relationship between this kind of ultrafast nonreciprocity effect and molecular orbital symmetry. This study broadens our understanding of nonreciprocal physical mechanisms in the field of strong-field ultrafast dynamics, and provides a theoretical basis for the experimental investigation of the nonreciprocal phase shift within the zeptosecond timescale in the response processes of matter under ultrafast laser irradiation.

Keywords: ultrafast nonreciprocal effect, zeptosecond, ultrafast laser, strong field

PACS: 42.65.Re, 87.15.ht, 87.15.mn

DOI: 10.1088/1674-1056/adf1e8 **CSTR:** 32038.14.CPB.adf1e8

1. Introduction

Photoionization is a fundamental quantum process that has proven to be a powerful tool in studying atoms, molecules, liquids, and solids. The ultrafast time-resolved measurement of photoionization has been a prominent and ongoing topic in the field of physics. Numerous studies have focused on the ultrafast electron dynamics during the process of photoionization. For instance, attosecond experimental techniques and relevant tunneling-time discussions have garnered significant attention.[1–4] Energy streaking methods have been employed to explore the time delays in electron ionization from different atomic orbitals,[5,6] and ionization time-delay measurements have been extended to threshold ionization processes.[7,8] Specifically, high-harmonic generation and isolated sub-100-attosecond extreme ultraviolet (XUV) pulses have provided a broad stage for investigating ultrafast physics with extremely high time resolution.[9,10] As a technological application, the attosecond dynamics of photoelectrons have received broad attention and research. For instance, the ultrashort XUV pulse is used as a precise trigger to time electronic ionization, and the corresponding time is recorded with a weak near-infrared (NIR) field, thereby creating an attosecond streaking camera.[11–14] Additionally, molecular attosecond photoelectron diffraction (MAPD) is a fascinating ultrafast imaging technique that also utilizes the interaction between XUV pulses and molecules.[15–22]

In molecular systems, characterized by more complex structures, the electron photoionization dynamics are closely related to chemical reactions and biological processes. Exploring ultrafast dynamics in molecular systems holds significant importance. In recent years, researchers have directed their attention towards questions about the timing in photoionization of extended systems, namely, the temporal buildup of the photoelectron wave across its spatially extended source. This means that laser-space propagation will play an important role, that is, the nondipole effect that cannot be ignored when discussing the molecular photoelectron angular distribution.[23] To observe such ultrafast processes, an electron interferometric technique has been employed, considering the nondipole propagation effect of light, leading to the detection of a zeptosecond time delay.[24,25] This experimental approach, pioneered by Grundmann *et al.*,[25] allows for the observation of physical processes occurring on an extremely small timescale. This time delay is interpreted as the travel time of the photon across the molecule.

To elaborate, when theory goes beyond the dipole approximation, one finds that there is a finite time delay for the interaction of a photon with different electron wave packets in a molecule, attributed to the finite speed of light. The corresponding escape-time difference manifests as a phase shift of the electron wave in the far field. The resulting phase shift in the interference structure can be experimentally observed,

†Corresponding author. E-mail: benshuai@hainanu.edu.cn

© 2025 Chinese Physical Society and IOP Publishing Ltd. All rights, including for text and data mining, AI training, and similar technologies, are reserved.

enabling the determination of the time taken by a photon to traverse a molecule, referred to as the zeptosecond delay (approximately 247 zeptoseconds for a hydrogen molecule).

To facilitate investigations, researchers have also utilized single ionization of H_2^+ as a model system for comprehending molecular ionization and dissociation.[26] Their calculations revealed a birth time delay of photoemission from the two nuclei, which amounted to several hundred zeptoseconds, qualitatively consistent with the experimental findings of Grundmann *et al.*[25] Traditionally, it has been assumed that electron wave packets are emitted from the central positions of the atomic cores. However, the separation between the two emission positions can deviate from the nuclear separation.[27,28] Lai *et al.*[29] discussed the influence of this deviation on the zeptosecond time delay. Additionally, Liu *et al.*[30] investigated how two types of nondipole effects impact the double-slit interference in single-photon ionization of H_2^+, particularly when the XUV pulse propagates in different directions. The nondipole effect stemming from individual atoms introduces a tilted envelope to the overall interference pattern, whereas the interaction delay between the pulse and the two nuclear centers further modifies the positions of interference maxima and minima.[26,31,32] The multielectron system model has also been carefully investigated, which includes the electron-electron correlation effects.[31,33] Moreover, studies have also focused on retrieving attosecond time delays and phase information from asymmetric molecules.[34]

The majority of the relevant studies are based on symmetric and simple systems, such as hydrogen molecules or hydrogen molecular ions, where the initial ionization phase difference is zero. In asymmetric systems, what is the response of the photoionization time delay to the phase shift of the electron wave in the far field? When photons traverse a heteronuclear molecule in different directions, they arrive at nuclei of different species at different times, resulting in more diverse ultrafast dynamics of photoionization. In our following investigation, we demonstrate that when considering asymmetric systems and incorporating the additional phase shift caused by laser propagation, the interference patterns in the photoelectron momentum spectra exhibit nonequivalent responses to different laser propagation processes. We define this asymmetric response phenomenon as an ultrafast nonreciprocity effect. Importantly, it is revealed in the following analysis that the ionization dynamics involved in the photoelectron phase shift shows zeptosecond temporal resolution.

Broadly speaking, nonreciprocity refers to a physical process exhibiting nonequivalent responses to input signals in opposite directions, demonstrating irreversibility or asymmetry. It finds extensive applications in various fields. For instance, in the research field of optical devices, the pioneering work of Gong *et al.*[35] on nonreciprocal transmission of optical fields and unidirectional amplification of optical fields[36] serves as a paradigm for the study of nonreciprocal optical devices. In this paper, we transplant analogous nonreciprocity concepts into the realm of ultrafast molecular photoionization, where we discuss the time delay of photoionization as photons traverse heteronuclear molecules and interact with the center of asymmetric electron wave packets. The rest of the paper is organized as follows. In Section 2, we introduce the numerical method. The results and analyses are presented in Section 3. The paper ends with a conclusion in Section 4. Atomic units (a.u.) are used unless stated otherwise.

2. Numerical methods

To simulate the photoionization process in the XUV pulse, we numerically solve the two-dimensional time-dependent Schrödinger equation (2D-TDSE) with the single-active-electron (SAE) approximation. The TDSE with dipole approximation reads

$$\mathrm{i}\frac{\partial}{\partial t}\Psi(\boldsymbol{r},t) = H(\boldsymbol{r},t)\Psi(\boldsymbol{r},t), \tag{1}$$

where $\boldsymbol{r} = (x,y)$ denotes the electron position in the (x,y) plane. Below we assume the molecular axis is aligned in the x direction. The Hamiltonian $H(\boldsymbol{r},t)$ is given by

$$H(\boldsymbol{r},t) = -\frac{1}{2}\nabla^2 + V(\boldsymbol{r}) + \boldsymbol{r}\cdot\boldsymbol{E}(t), \tag{2}$$

$$\boldsymbol{A}(t) = -A_0 \sin^2\left(\frac{\omega t}{2N}\right)\sin(\omega t)\cdot\boldsymbol{n}, \tag{3}$$

$$\boldsymbol{E}(t) = -\frac{\partial}{\partial t}\boldsymbol{A}(t), \tag{4}$$

where $\boldsymbol{A}(t)$ is the vector potential and $\boldsymbol{E}(t)$ is the electric field. A_0 and ω are the amplitude and angular frequency, respectively. $\boldsymbol{n}$ is the unit vector in the polarization direction. The laser intensity is chosen to be 5.0×10^{15} W/cm^2. We use an $N = 20$ cycle linearly polarized XUV pulse with a wavelength of 3.5 nm ($\omega = 13$ a.u.). The effective screened potential is in the form of[18]

$$V(\boldsymbol{r}) = -\sum_j \frac{Z_j}{\sqrt{\boldsymbol{r}_j^2 + a_j^2}}, \tag{5}$$

where the subscript j labels the nuclei at fixed positions $\boldsymbol{\rho}_j$ and $\boldsymbol{r}_j = \boldsymbol{r} - \boldsymbol{\rho}_j$. Z_j denotes the nuclear charge of nucleus j. The soft-core parameter a_j is tuned to correctly reproduce the orbital shape and state energy of the molecule. The Crank–Nicolson method[37,38] on a Cartesian grid is used to numerically solve the 2D-TDSE. The initial wave function is prepared by imaginary-time propagation.[39] Due to the linearity of the Schrödinger equation, for real-time propagation we split the electron wave function $\Psi(t)$ at any given time t into two parts[40]

$$\Psi(t) = \Psi(t)(1 - F_\mathrm{s}(r_\mathrm{c})) + \Psi(t)F_\mathrm{s}(r_\mathrm{c}) = \Psi_\mathrm{i}(t) + \Psi_\mathrm{o}(t), \tag{6}$$

where $F_{\rm s}(r_{\rm c}) = 1/\left[1+{\rm e}^{-(r-r_{\rm c})/\beta}\right]$ is an absorbing function that separates the propagation space into the inner and outer parts, smoothly. $\Psi_i(t)$ propagates under the full Hamiltonian in the inner space, and $\Psi_{\rm o}(t)$ propagates under the Volkov Hamiltonian in the outer space analytically, which represents the ionized part.[40,41] Then we calculate

$$\Phi(\boldsymbol{p},t) = \int \Psi_{\rm o}(t)\,\frac{1}{2\pi}\,{\rm e}^{-{\rm i}(\boldsymbol{p}+\boldsymbol{A}(t))\cdot\boldsymbol{r}}\,{\rm d}^2\boldsymbol{r}, \tag{7}$$

with $\tilde{\Phi}(\boldsymbol{p},t) = \exp\left[-{\rm i}\int_t^{\infty}\frac{1}{2}\left(\boldsymbol{p}+\boldsymbol{A}(t)\right)^2{\rm d}t\right]\Phi(\boldsymbol{p},t)$. Finally, we obtain the electron momentum spectrum by

$$\frac{{\rm d}^2P(\boldsymbol{p})}{{\rm d}E\,{\rm d}\theta} = \left|\sum_t \tilde{\Phi}(\boldsymbol{p},t)\right|^2, \tag{8}$$

where $E = |\boldsymbol{p}|^2/2$ is the electron energy and θ is the angle of the emitted electron. The time step of propagation is $\Delta t = 0.2$ a.u. At the end of the laser pulse, the wave function is propagated for a sufficiently long time to collect "slow" electrons.[42] The space ranges from -819.2 a.u. to 819.2 a.u. in both directions with a grid size of $\Delta x = \Delta y = 0.2$ a.u. The boundary of the inner space is $r_{\rm c} = 130$ a.u. with $\beta = 6.0$ a.u. We take into consideration that the speed of light is much greater than the velocity of photoelectrons. Therefore, when the electron reaches the absorption boundary at the distance of $r_{\rm c}$, it is assumed that the XUV light has propagated far enough, and thus the laser pulse is considered to have ceased. Consequently, when considering the nondipole effect, the propagation of $\Psi_{\rm o}(t)$ analytically follows the Volkov Hamiltonian in the outer space and remains valid.

When discussing the nondipole propagation effect of the laser, it suffices to replace the time variable t with the light-cone time $\eta = t - n(x-a_0)/c$, and Hamiltonian (2) should be rewritten in the Göppert–Mayer gauge with accuracy up to order $1/c$[43,44]

$$H(\boldsymbol{r},\eta) = -\frac{1}{2}\nabla^2 + \boldsymbol{r}\cdot\boldsymbol{E}(\eta)\left(1-n\frac{\hat{p}_x}{c}\right) + V(\boldsymbol{r}), \tag{9}$$

where $n = +1$ and -1 represent the propagation of the laser along the $+x$ and $-x$ directions (or $+y$ and $-y$ directions), respectively, and $n = 0$ corresponds to the results obtained under the dipole approximation. Here, a_0 denotes the initial distance between the pulse and the molecule.

The method of determining time delay is based on the electron interferometric technique. To elaborate, the two nuclei (or two emitting sites) act as "slits" in the microscopic double-slit experiment, and the photoelectron momentum distribution (PMD) exhibits a two-center interference pattern.[45–55] In general, this kind of interference can be obtained by superposition of the phase term of the electron wave packet emitted from the $N_{\rm c}$ centers

$$\sum_{j=1}^{N_{\rm c}} \varepsilon_j A_j\,{\rm e}^{{\rm i}\left[\boldsymbol{p}\cdot\left(\boldsymbol{r}-\boldsymbol{R}_j\right)+\phi_j\right]}, \tag{10}$$

with momentum $\boldsymbol{p}$ emerging from the j-th center with position vector $\boldsymbol{R}_j$, initial phase ϕ_j, and amplitude A_j. $\varepsilon_j = 1$ and -1 correspond to electrons emerging from molecular orbitals of ungerade and gerade symmetries, and also correspond to symmetric bonding and antisymmetric antibonding orbitals. For the two-center case, i.e., $N_{\rm c} = 2$, the interference feature can be written as

$$P \sim \begin{cases} \cos^2\left(\boldsymbol{p}\cdot\frac{\boldsymbol{R}}{2}+\frac{\Delta\phi}{2}\right), & \varepsilon_1 = \varepsilon_2 = 1, \\ \sin^2\left(\boldsymbol{p}\cdot\frac{\boldsymbol{R}}{2}+\frac{\Delta\phi}{2}\right), & \varepsilon_1 = -\varepsilon_2 = 1, \end{cases} \tag{11}$$

$\Delta\phi = \phi_1 - \phi_2$ is the initial phase difference between the two waves. When the electron birth time delay due to the nondipole effect is considered, the relationship between the phase shift and the time delay is given by

$$2\pi\left(\frac{\cos(\alpha_0)R_{\rm w}}{\lambda_{\rm de}} - \frac{t_{\rm d}v_{\rm ph}}{\lambda_{\rm de}}\right) = 0. \tag{12}$$

Here, $\lambda_{\rm de}$ is the electron's de Broglie wavelength, and $v_{\rm ph}$ represents the phase velocity, which can be estimated as $v_{\rm ph} = p_{\rm e}/2$ under non-relativistic conditions. The angle α_0 is the photoelectron momentum direction with respect to the molecular axis.

3. Results

To elucidate the asymmetric characteristics of the PMD interference structure for asymmetric molecules under both the dipole approximation and when considering nondipole laser propagation, we perform simulations for symmetric molecular systems (H_2^+) and asymmetric molecular systems (HeH^{2+}). For HeH^{2+}, the internuclear distance is set to $R_0 = 4$ a.u., consistent with commonly adopted parameters in previous studies.[56] For comparative purposes, the nuclear separation of H_2^+ is also set to $R_0 = 4$ a.u.

From the potential energy curve of the $1s\sigma$ state of the hydrogen molecular ion, the ionization potential at $R_0 = 4$ a.u. is $I_{\rm p} = 0.7956$ a.u. The corresponding charge parameters are $Z_1 = Z_2 = 1$, and the softening parameters are $a_1 = a_2 = 0.8465$. The laser is assumed to propagate along the x direction, with polarization along the y direction, i.e., $\boldsymbol{n} = (0,1)$. The calculated coordinate-space wave function of the $1s\sigma$ initial state is shown in Fig. 1(a). It represents a symmetric bonding orbital with a clear two-center structure, arising from the double Coulomb potential well of the molecule. The relatively large internuclear distance further enhances the spatial localization of the electronic wave packet compared with the equilibrium nuclear separation of the ground state. Consequently, under XUV excitation, the PMDs exhibit a distinct two-center interference structure.

Figures 1(c)–1(e) present the PMDs for photoelectrons with momentum magnitude $p_{\rm e} = 4.9$ a.u. Figure 1(c) shows

the dipole approximation result ($n = 0$). Owing to the bonding orbital symmetry with $\varepsilon_1 = \varepsilon_2 = 1$, the interference maximum is located at the center of the momentum spectrum ($p_x = 0$), consistent with Eq. (11). Furthermore, due to the intrinsic molecular symmetry, the PMDs are symmetric and this is more evident in the corresponding photoelectron angular distribution (PAD) in the molecular frame (Fig. 1(b), dashed line).

From the PMDs, the interference fringe spacing in momentum space is determined to be $\Delta p_x = 1.56$ a.u. According to Eq. (11), the effective separation between electron emission positions is $R_w = 2\pi/\Delta p_x = 4.03$ a.u., which is in close agreement with the chosen internuclear distance $R_0 = 4$ a.u. This result confirms that at relatively large internuclear separations, the electron emission sites localize near the nuclei, in contrast with bonding orbitals at equilibrium separation, where electron density is concentrated between the two nuclei.[29]

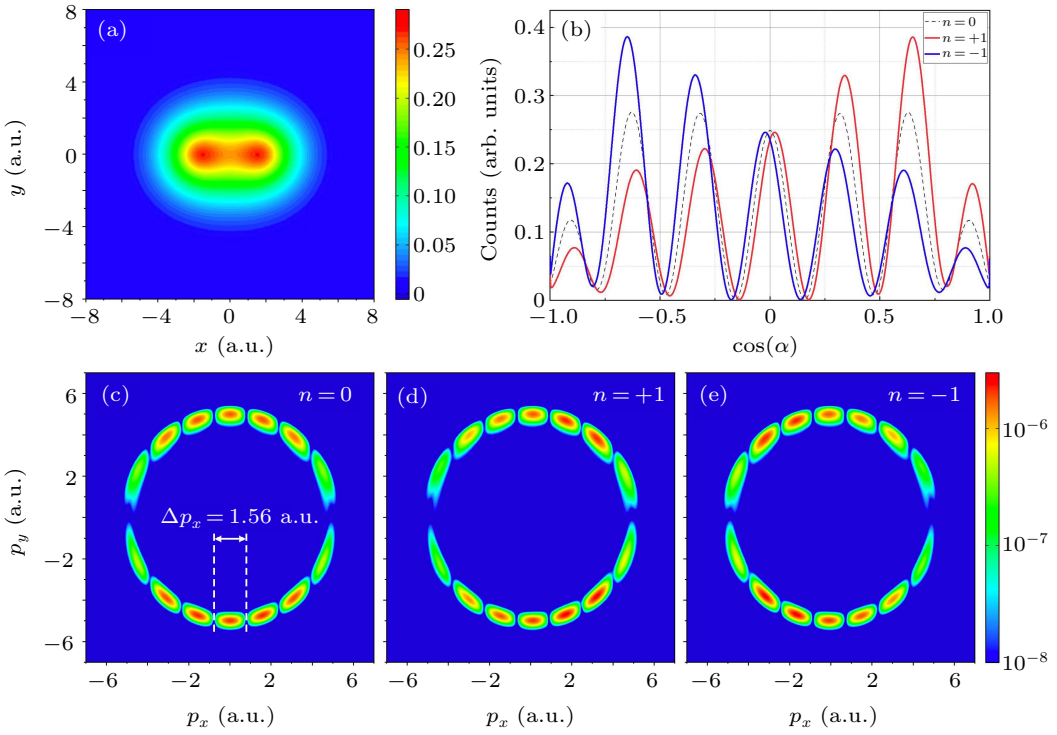


Fig. 1. (a) Wave functions of the ground state of H_2^+. (b) The corresponding radially integrated PADs, i.e., cos(α), where the angle α is the photoelectron momentum direction with respect to the molecular axis. The dashed line denotes the PAD in the dipole approximation case, while the red solid line and the blue solid line represent the PAD for the laser propagating along the $+x$ and $-x$ directions, respectively. (c) Simulated molecule-frame PMD of H_2^+ in the dipole approximation. (d) and (e) Simulated molecule-frame PMD of H_2^+ with the laser propagating along the $+x$ direction and $-x$ direction, respectively.

It is more important to focus on the nondipole propagation effects of the laser, where the XUV pulse propagating through the distance of R_w leads to an initial ionization time delay for electrons emitted from the two centers of the molecule. The theoretical delay should be $R_w/c = 0.02941$ a.u., approximately 712 zeptoseconds, where c represents the speed of light. This time delay introduces an additional initial phase difference to the electron wave packets emitted from the two centers, resulting in observable phase shifts in the momentum spectra interference structure, as shown in Figs. 1(d) and 1(e). Figure 1(d) displays the PMD when the laser propagates along the $+x$ direction, i.e., $n = +1$. In this case, the ionization time of the electron wave packet from the right center is delayed compared to that from the left center due to the finite speed of light, resulting in a rightward shift of the interference fringes with a phase shift of $\cos(\alpha_0) = 0.018$. According to Eq. (12), when the laser propagates along the $+x$ direction ($n = +1$), the delay time for electron ionization from the right center compared to the left center is $t_d = 2R_w \cos(\alpha_0)/p_e = 0.02937$ a.u., which is close to the expected value of R_w/c. Similarly, when the laser propagates along the $-x$ direction ($n = -1$), it causes a leftward shift of the interference fringes (Fig. 1(e)), with a phase shift of $\cos(\alpha_0) = -0.018$ and $t_d = -0.02937$ a.u. (the negative sign indicates a delay in electron ionization from the left center compared to the right center). From the PAD curves, represented by the solid red and blue lines in Fig. 1(b), it can be clearly observed that the phase shifts corresponding to laser propagation in different directions are symmetric. This symmetry arises from the inherent symmetry of the system and the spatial symmetry of the system's response to laser propagation. Ultrafast dynamical phenomena are therefore considered equivalent for forward and backward laser propagation. In this paper, we define this situation as reciprocity, which manifests on the temporal scale of hundreds of zeptoseconds.

Next, we discuss the case of the heteronuclear HeH^{2+} ion.

First, we consider the initial state to be the 1sσ state. The ionization potential of the ground state is 2.2506 a.u. Here, we use the parameters of $Z_1 = 1$, $Z_2 = 2$, and $a_1 = a_2 = 0.398$ a.u. The wave function of the initial state orbital is shown in Fig. 2(a). Since the He nucleus carries a charge of +2, it attracts electrons more strongly than the H nucleus. Therefore, in the ground state, the electron is mainly localized near the He nucleus, and the orbital exhibits almost no two-center structural features. In the PMD, as shown in Fig. 2(c), there is similarly almost no evidence of two-center interference fringes, and the results are very close to those of a single atom. In this situation, when the laser propagates from both the positive and negative directions along the molecular axis and interacts with the molecule, the PMD is shifted as a whole toward the laser propagation direction due to momentum transfer from the photon to the photoelectron,[57–59] as shown in Figs. 2(d) and 2(e). The influence of laser propagation can be observed more clearly from the PADs (Fig. 2(b)). The overall distribution of the curves also resembles the atomic case, exhibiting a high degree of symmetry.

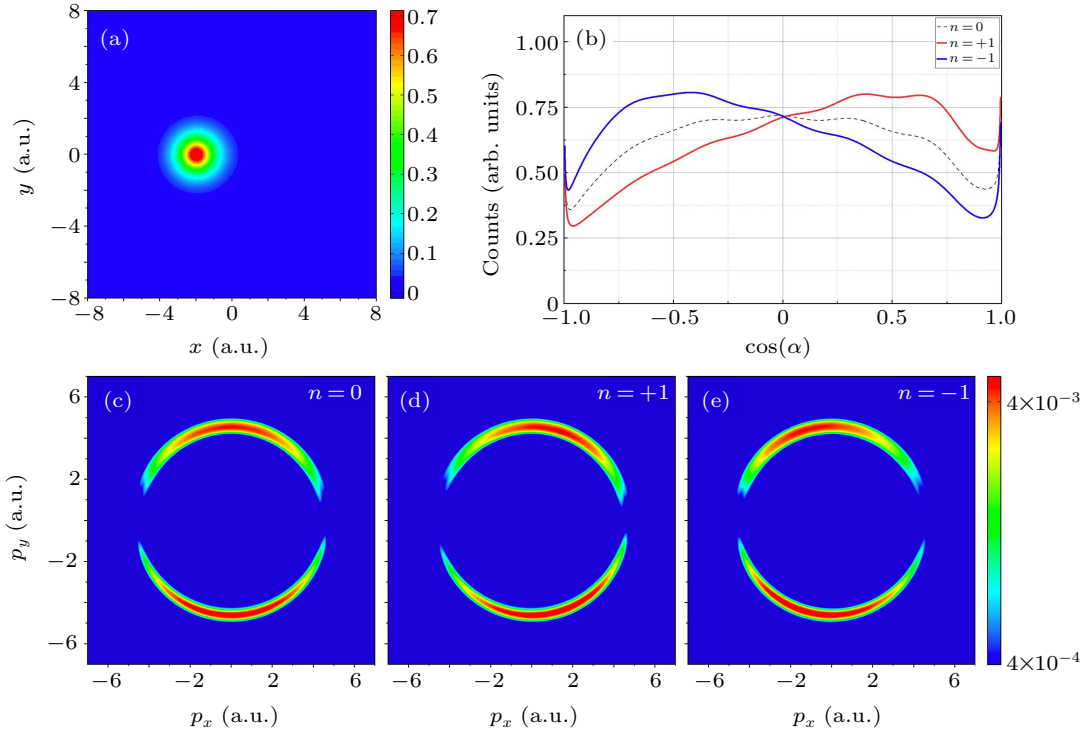


Fig. 2. (a) Wave functions of the 1sσ state of HeH^{2+}. (b) The corresponding radially integrated PADs. The dashed line denotes the PAD in the dipole approximation case, while the red solid line and the blue solid line represent the PAD for the laser propagating along the $+x$ and $-x$ directions, respectively. (c) Simulated molecule-frame PMD of HeH^{2+} in the dipole approximation. (d) and (e) Simulated molecule-frame PMDs of HeH^{2+} with the laser propagating along the $+x$ direction and $-x$ direction, respectively.

According to the Schmidt orthogonalization method,[60] a series of mutually orthogonal excited states can be obtained. Among them, the 2pσ excited state is shown in Fig. 3(a), where the initial state exhibits an asymmetric antibonding orbital with two-center structure characteristics. Furthermore, the corresponding wave function exhibits greater localization near the H nucleus, which is qualitatively consistent with results reported in previous research.[56,61] When the XUV pulse interacts with the excited-state orbital system possessing a two-center structure, the photoelectron momentum spectrum exhibits two-center interference fringes, as shown in Figs. 3(c)–3(e). Figure 3(c) represents the dipole approximation result for $n = 0$, where the photoelectron momentum magnitude is approximately $p_e = 4.64$ a.u. Interference minima are also observed near the center of the momentum spectrum ($p_x = 0$), which is attributed to the antisymmetric initial wave function of the first excited state ($\varepsilon_1 = -\varepsilon_2 = 1$). Moreover, the fringe spacing is $\Delta p_x = 1.45$ a.u., and based on Eq. (11), the separation of the electron emission positions is $R_w = 2\pi/\Delta p_x = 4.33$, slightly larger than the internuclear separation R_0. This is due to the fact that the electron wave packet in the antibonding orbital exhibits a tendency for mutual repulsion, which is consistent with previous findings.[29]

Careful observation of the momentum spectra in the dipole approximation (Fig. 3(c)), combined with examination of the PAD (gray dashed line in Fig. 3(b)), reveals that the interference minimum near the center of the momentum spectrum is not exactly located at $p_x = 0$. Instead, it is slightly shifted to the left. This shift is due to the inherent asymmetry of the system, even in the absence of any time delay between the laser and the center of interaction. The initial ionization phase difference $\Delta\phi$ is no longer zero, which is related

to the different energy states and the attractive force exerted by the nuclei on the electron wave packets localized near different centers. Considering the structural characteristics of this asymmetric system, when the nondipole propagation effects of the laser are further taken into account, the interference response in the momentum spectra caused by the finite speed of light differs for forward and backward laser propagation directions. Figure 3(d) shows the result of laser propagation along the $+x$ direction ($n=+1$), where the phase shift induced by the ionization time delay causes the interference fringes to shift to the left. This shift largely compensates for the effect of the initial phase difference $\Delta\phi$ and ultimately brings the interference minima closer to the central position ($p_x=0$). This is similar to the conclusion in Ref. [34]. However, our focus here is on the nonreciprocal effects arising from laser pulses propagating in opposite directions.

On the other hand, figure 3(e) shows the result of laser propagation along the $-x$ direction ($n=-1$), where the interference phase shift shifts to the right. The effect of the initial phase difference $\Delta\phi$ is determined by the structural characteristics of the system and is independent of the propagation direction of the external field. Therefore, the interference minima are shifted further to the right, away from the central region. This characteristic is more clearly demonstrated in the PAD distribution shown in Fig. 3(b) by the solid red and blue lines, indicating an asymmetric response of the interference structure to laser propagation in both forward and backward directions. Thus, it exhibits nonreciprocity.

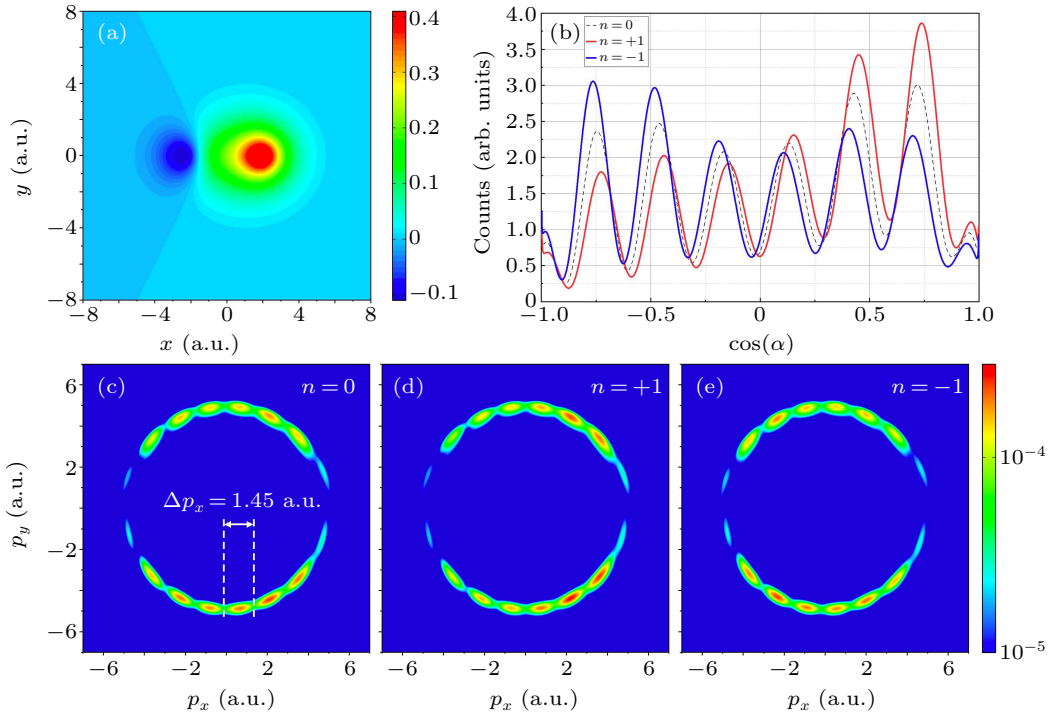


Fig. 3. (a) Wave functions of the 2pσ excited state of HeH^{2+}. (b) The corresponding radially integrated PADs. The dashed line denotes the PAD in the dipole approximation case, while the red solid line and the blue solid line represent the PAD for the laser propagating along the $+x$ and $-x$ directions, respectively. (c) Simulated molecule-frame PMD of HeH^{2+} in the dipole approximation. (d) and (e) Simulated molecule-frame PMDs of HeH^{2+} with the laser propagating along the $+x$ direction and $-x$ direction, respectively.

The phase shift of the solid red and blue lines in Fig. 3(b) relative to the dashed line reveals $\cos(\alpha_0)=\pm 0.0169$. Using Eq. (12), it can be deduced that $t_{\rm d}=2R_{\rm w}\cos(\alpha_0)/p_{\rm e}=\pm 0.0316$ a.u., which corresponds to a time delay of approximately 764 zeptoseconds, in agreement with the expected value of $R_{\rm w}/c$. This result clearly demonstrates the inequivalence of molecular photoionization in different propagation directions under ultrafast time resolution, indicating the nonreciprocal effect in ultrafast dynamics.

Furthermore, for comparison and further analysis, we have also calculated the case of the 2pπ state of HeH^{2+}. Figure 4(a) displays the molecular orbital of the 2pπ state, where the two-center structure is arranged along the perpendicular molecular axis and exhibits the same localization as an antibonding orbital ($\varepsilon_1=-\varepsilon_2=1$). The laser propagation is set along the y direction with $\eta=t-n(y-a_0)/c$, and the polarization is along the x direction, that is $\boldsymbol{n}=(1,0)$. The operator $\hat{p}_x$ in Eq. (9) should also be changed to $\hat{p}_y$. In this case, the two-center interference in the PMDs manifests along the y direction, and the central region ($p_y=0$) still exhibits interference minima, as shown in Fig. 4(c), which corresponds to the dipole approximation result. When considering laser propagation along the $+y$ and $-y$ directions, the photoelectron momentum spectra undergo a phase-shifted response in the y direction, causing the interference minima to shift upward and downward, as shown in Figs. 4(d) and 4(e). Due to

the identical localization of the electron wave packets in the two-center region, the resulting phase shifts remain identical. From the PAD in Fig. 4(b), it can be clearly observed that the interference structure in the momentum spectra along the y direction exhibits symmetric responses to laser propagation in both forward and backward directions (position of the solid red and blue lines relative to the dashed line), similar to the case of H_2, and thus does not exhibit nonreciprocity. These results further indicate that ultrafast nonreciprocity is closely related to the asymmetry of the initial molecular orbitals.

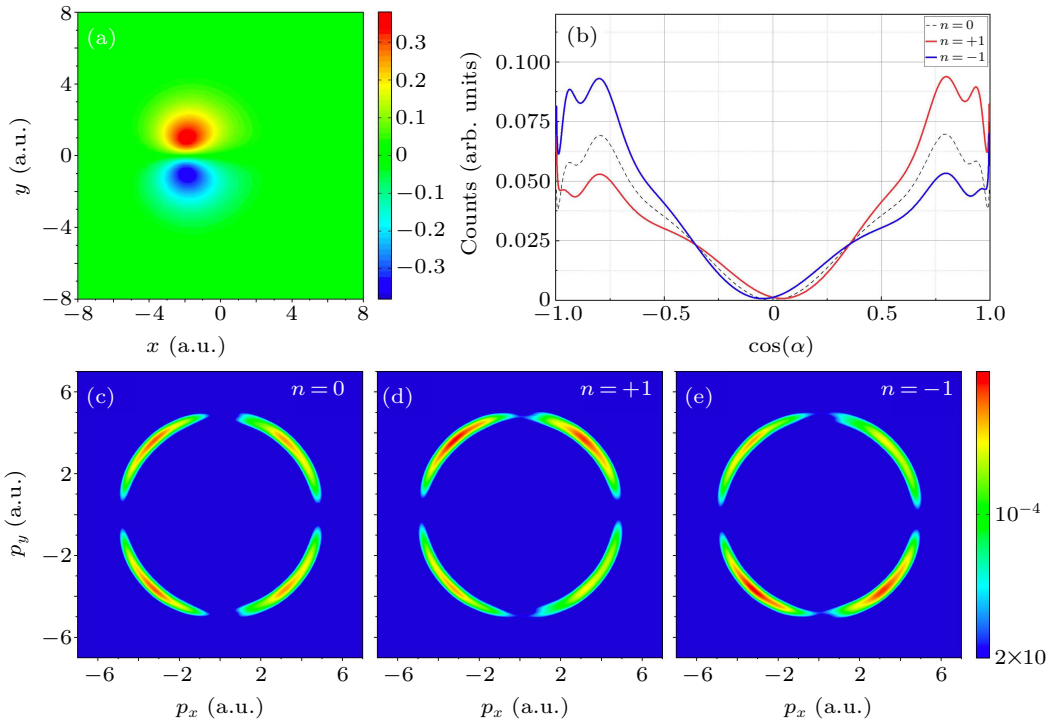


Fig. 4. (a) Wave functions of the 2pπ excited state of HeH^{2+}. (b) The corresponding radially integrated PADs. The dashed line denotes the PAD in the dipole approximation case, while the red solid line and the blue solid line represent the PAD for the laser propagating along the $+y$ and $-y$ directions, respectively. (c) Simulated molecule-frame PMD of HeH^{2+} in the dipole approximation. (d) and (e) Simulated molecule-frame PMDs of HeH^{2+} with the laser propagating along the $+y$ direction and $-y$ direction, respectively.

The above research illuminates the response characteristics of molecular strong field photoionization processes to laser propagation in different directions under ultrafast time resolution. The initial ionization phase difference of the system and the additional phase difference caused by the finite-speed-of-light-induced ionization time delay together determine the phase shift of the two-center interference in the photoelectron momentum spectrum. The initial phase difference of the system itself is not affected by the direction of external field propagation, and its contribution to the phase shift is fixed. The ionization-delay-induced additional phase difference caused by laser propagation is closely related to the propagation direction, which directly leads to different directions of interference fringe movement. Therefore, when the system has an asymmetric initial two-center, the total phase shift will exhibit different responses under the action of laser propagation in different directions, that is, ultrafast nonreciprocity. When the system is of a symmetric structure, there is no initial phase $\Delta\phi$, and the delay-induced additional phase difference caused by laser propagation makes the interference fringes have the same phase shift relative to the central position in PAD, resulting in symmetry, with no nonreciprocal effect, as in the case of the H_2^+ and the 2pπ excited state of HeH^{2+}.

4. Conclusion

In summary, by comparing the interference phase shifts in the photoelectron momentum spectra of symmetric and asymmetric systems under strong field conditions, we have elucidated the mechanism of a zeptosecond nonreciprocal phase shifter in molecules under strong field interactions. The discussed findings present significant opportunities for further research. For instance, in experimental settings, HeH^{2+} ions can be prepared in different state mixtures (e.g., ground state and 1sσ state) and exhibit time-periodic oscillations associated with energy differences.[62,63] Through the ultrafast nonreciprocal effect, the response of dynamically evolving systems to light propagation can be investigated with a time resolution of several hundred zeptoseconds. Additionally, research indicates that double-slit interference occurs in ion momentum spectra associated with molecular dissociation through the photoelectron-ion entanglement, and is strongly correlated with the photoelectron emission angle. Therefore, the laser propagation direction dependence proposed in this study will

further influence the photoelectron emission direction, thereby affecting the interference phase shift in ion momentum. For heteronuclear molecules, the difference in atomic masses may also introduce additional nonreciprocal effects.[64] Therefore, a wider variety of polar molecules with more complex molecular orbital structures can display richer nonreciprocal patterns in response to ultrafast lasers through multiple ionization channels, revealing additional ultrafast physical processes. The findings of this research provide a theoretical basis for experimental investigations of strong field ultrafast nonreciprocity in photoelectron dynamics.

This study also presents certain possibilities for application in the field. In the fabrication of nonreciprocal devices such as isolators and circulators, the nonreciprocal temporal phase shifter plays a crucial role. By utilizing the structural characteristics and rational design and assembly of reciprocal and nonreciprocal components, controlled constructive or destructive interference can be achieved at different output ports through the interference principles of light, enabling directed transmission of light.[65] Drawing an analogy to these nonreciprocal devices, we transplant this concept into the realm of ultrafast optoelectronic dynamics research. With strong field interactions, the two-center interference of molecular photoelectrons also carries phase information of electron wave packets, while the finite-speed response of light propagation induces phase shifts. Therefore, we can naturally interpret this process as a novel phase shifter for optoelectronic properties, referred to as a photoelectron phase shifter, which exhibits reciprocal and nonreciprocal characteristics influenced by molecular symmetry. The abundance of molecular species in nature results in diverse interference patterns, offering greater opportunities for the research and application of ultrafast photoelectron phase shifters.

Acknowledgments

Project supported by the National Natural Science Foundation of China (Grant No. 12204136) and the Hainan Provincial Natural Science Foundation of China (Grant No. 122QN217).

References

[1] Eckle P, Pfeiffer A N, Cirelli C, Staudte A, Dorner R, Muller H G, Buttiker M and Keller U 2008 *Science* **322** 1525
[2] Rost J M and Saalmann U 2019 *Nat. Photon.* **13** 439
[3] Ramons R, Spierings D, Racicot I and Steinberg A 2020 *Nature* **583** 529
[4] Tong J H, Liu X, Dong W, Jiang W, Zhu M, Xu Y, Zuo Z, Lu P, Gong X, Song X, Yang W and Wu J 2022 *Phys. Rev. Lett.* **129** 173201
[5] Schultze M, Fiess M, Karpowicz N, *et al.* 2010 *Science* **328** 1658
[6] Isinger M, Squibb R J, Busto D, Zhong S, Harth A, Kroon D, Nandi S, Arnold C L, Miranda M, Dahlström J M, Lindroth E, Feifel R, Gisselbrecht M and L'Huillier A 2017 *Science* **358** 893
[7] Zipp L, Natan A and Bucksbaum P 2014 *Optica* **1** 361
[8] Song X H, Shi G, Zhang G J, Xu J W, Lin C, Chen J and Yang W F 2018 *Phys. Rev. Lett.* **121** 103201
[9] Krausz F and Ivanov M 2009 *Rev. Mod. Phys.* **81** 163
[10] Chang Z and Corkum P 2010 *J. Opt. Soc. Am. B* **27** B9
[11] Hentschel M, Kienberger R, Spielmann C, Reider G A, Milosevic N, Brabec T, Corkum P, Heinzmann U, Drescher M and Krausz F 2001 *Nature* **414** 509
[12] Itatani J, Quéré F, Yudin G L, Ivanov M Yu, Krausz F and Corkum P B 2002 *Phys. Rev. Lett.* **88** 173903
[13] Kitzler M, Milosevic N, Scrinzi A, Krausz F and Brabec T 2022 *Phys. Rev. Lett.* **88** 173904
[14] Pazourek R, Nagele S and Burgdörfer J 2015 *Rev. Mod. Phys.* **87** 765
[15] Zuo T, Bandrauk A D and Corkum P B 1996 *Chem. Phys. Lett.* **259** 313
[16] Hu S X, Collins L A and Schneider B I 2009 *Phys. Rev. A* **80** 023426
[17] Krasniqi F, Najjari B, Strüder L, Rolles D, Voitkiv A and Ullrich J 2010 *Phys. Rev. A* **81** 033411
[18] Li Y, Qin M, Zhu X, Zhang Q, Lan P and Lu P 2015 *Opt. Express* **23** 10687
[19] Nguyen N T, Lucchese R R, Lin C D and Le A T 2016 *Phys. Rev. A* **93** 063419
[20] Minemoto S, Teramoto T, Akagi H, Fujikawa T, Majima T, Nakajima K, Niki K, Owada S, Sakai H, Togashi T, Tono K, Tsuru S, Wada K, Yabashi M, Yoshida S and Yagishita A 2016 *Sci. Rep.* **6** 38654
[21] Kastirke G, Markus S, Weller M, *et al.* 2020 *Phys. Rev. X* **10** 021052
[22] Sun Z, Yao H, Ren X, Liu Y, Wang D, Zhao W, Wang C and Yang C 2021 *Opt. Express* **29** 10893
[23] Hosaka H, Adachi J, Golovin A V, Takahashi M, Teramoto T, Watanabe N, Yagishita A, Semenov S K and Cherepkov N A 2006 *J. Phys. B: At. Mol. Opt. Phys.* **39** L25
[24] Wang M X, Chen S G, Liang H and Peng L Y 2020 *Chin. Phys. B* **29** 013302
[25] Grundmann G, Trabert D, Fehre K, Strenger N, Pier A, Kaiser L, Kircher M, Weller M, Eckart S, Schmidt L Ph H, Trinter F, Jahnke T, Schöffler M S and Dörner R 2020 *Science* **370** 339
[26] Zhang Z H and He F 2021 *Phys. Rev. A* **103** 033112
[27] Seideman T, Ivanov M Y and Corkum P B 1995 *Phys. Rev. Lett.* **75** 2819
[28] Zuo T and Bandrauk A D 1995 *Phys. Rev. A* **52** R2511
[29] Lai X, Xu S, Yu S, Shi M, Quan W and Liu X 2021 *Phys. Rev. A* **104** 043105
[30] Liu K, Hu Y, Zhang Q and Lu P 2021 *Opt. Express* **29** 38758
[31] Liang H, Grundmann S, Fang Y, Geng L, Gong Q and Peng L 2021 *Phys. Rev. A* **104** L021101
[32] He P L, Hatsagortsyan K Z and Keitel C H 2022 *Phys. Rev. Lett.* **128** 183201
[33] Hu Y, Liu K, Ma Q and Lu P 2022 *J. Opt. Soc. Am. B* **39** 2486
[34] Tian Y, Hu Y, Zhou Y, Lu P and Liu K 2024 *Phys. Rev. Research* **6** 043150
[35] Zhang S, Hu Y, Lin G, Niu Y, Xia K, Gong J and Gong S 2018 *Nat. Photonics* **12** 744
[36] Lin G, Zhang S, Hu Y, Niu Y, Gong J and Gong S 2019 *Phys. Rev. Lett.* **123** 033902
[37] Sudiarta W and Geldart D J W 2007 *J. Phys. A: Math. Theor.* **40** 1885
[38] Bian X B 2014 *Phys. Rev. A* **90** 033403
[39] Protopapas M, Keitel C H and Knight P L 1997 *Rep. Prog. Phys.* **60** 389
[40] Tong X M, Hino K and Toshima N 2006 *Phys. Rev. A* **74** 031405
[41] Tong X M, Watahiki S, Hino K and Toshima N 2007 *Phys. Rev. Lett.* **99** 093001
[42] He P L, Takemoto N and He F 2015 *Phys. Rev. A* **91** 063413
[43] Klaiber M, Yakaboylu E, Bauke H, Hatsagortsyan K Z and Keitel C H 2013 *Phys. Rev. Lett.* **110** 153004
[44] He P L, Klaiber M, Hatsagortsyan K Z and Keitel C H 2022 *Phys. Rev. A* **105** L031102
[45] Rolles D, Braune M, Cvejanović S, Geßner O, Hentges R, Korica S, Langer B, Lischke T, Prümper G, Reinköster A, Viefhaus J, Zimmermann B, McKoy V and Becker U 2005 *Nature* **437** 711
[46] Liu X J, Cherepkov N A, Semenov S K, Kimberg V, Gel'mukhanov F, Prümper G, Lischke T, Tanaka T, Hoshino M, Tanaka H and Ueda K 2006 *J. Phys. B: At. Mol. Opt. Phys* **39** 4801
[47] Akoury D, Kreidi K, Jahnke T, *et al.* 2007 *Science* **318** 949
[48] Zimmermann B, Rolles D, Langer B, Hentges R, Braune M, Cvejanovic S, Geßner O, Heiser F, Korica S, Lischke T, Reinköster A, Viefhaus J, Dörner R, McKoy V and Becker U 2008 *Nat. Phys.* **4** 649
[49] Schöffler M S, Kreidi K, Akoury D, *et al.* 2008 *Phys. Rev. A* **78** 013414

[50] Yang W, Sheng Z, Feng X, Wu M, Chen Z and Song X 2014 *Opt. Express* **22** 2519
[51] Kunitski M, Eicke N, Huber P, Köhler J, Zeller S, Voigtsberger J, Schlott N, Henrichs K, Sann H, Trinter F, Schmidt L, Kalinin A, Schöffler M S, Jahnke T, Lein M and Dörner R 2019 *Nat. Commun.* **10** 1
[52] Zhenning G and Liu Y 2020 *J. Phys. B: At. Mol. Opt. Phys.* **53** 065004
[53] Acharya B, Dubey S, Romans K, Silva A, Foster K, Russ O, Bartschat K, Douguet N and Fischer D 2022 *Phys. Rev. A* **106** 023113
[54] Heck S, Han M, Jelovina D, Ji J, Perry C, Gong X, Lucchese R, Ueda K and Wörner H 2022 *Phys. Rev. Lett.* **129** 133002
[55] Guo Z, Ge P, Fang Y, Dou Y, Yu X, Wang J, Gong Q and Liu Y 2022 *Ultrafast Sci.* **2022** 9802917
[56] Bian X B and Bandrauk A D 2012 *Phys. Rev. A* **86** 053417
[57] Lao D, He P L and He F 2016 *Phys. Rev. A* **93** 063403
[58] Huo Y N, Li J and Ma F C 2018 *Chin. Phys. B* **27** 013203
[59] Xu Z, Liang J, Liu K, Ciappina M F, Lu P and Zou Y 2024 *Phys. Rev. A* **110** 013124
[60] Strang G 2013 *Introduction to Linear Algebra* 5th Edn. (Université Paris-Dauphine)
[61] Campos J A, Nascimento D L, Cavalcante D T, Fonseca A L A and Nunes A O C 2006 *Int. J. Quantum Chem.* **106** 2587
[62] He M, Li Y, Zhou Y, Li M, Cao W and Lu P 2018 *Phys. Rev. Lett.* **120** 133204
[63] He M, Zhou Y, Tan J, Li Y, Li M and Lu P 2018 *J. Phys. B: At. Mol. Opt. Phys.* **51** 245602
[64] He P L, Hatsagortsyan K Z and Keitel C H 2023 *Phys. Rev. Lett.* **131** 013201
[65] Taravati S and Eleftheriades G V 2022 *Phys. Rev. Appl.* **18** 034082